

# The mass of the Milky Way and M31 using the method of least action

Steven Phelps

Physics Department, Technion, Haifa 32000, Israel

`steven@alumni.princeton.edu`

Adi Nusser

Physics Department and the Asher Space Science Institute-Technion, Haifa 32000, Israel

`adi@physics.technion.ac.il`

and

Vincent Desjacques

Departement de Physique Theorique and Center for Astroparticle Physics, Universite de  
Geneva, CH-1211 Geneva, Switzerland

`Vincent.Desjacques@unige.ch`

Received \_\_\_\_\_; accepted \_\_\_\_\_

## ABSTRACT

We constrain the most likely range of masses for the Milky Way and M31 using an application of the Numerical Action Method (NAM) that optimizes the fit to observed parameters over a large ensemble of NAM-generated solutions. Our 95% confidence level mass ranges,  $2.5 - 5.0 \times 10^{12} M_{\odot}$  for MW and  $1.0 - 5.0 \times 10^{12} M_{\odot}$  for M31, are consistent with the upper range of estimates from other methods and suggests that a larger proportion of the total mass becomes detectable when the peculiar motions of many nearby satellites are taken into account in the dynamical analysis. We test the method against simulated Local Group catalogs extracted from the Millennium Run to confirm that mass predictions are consistent with actual galaxy halo masses.

*Subject headings:* cosmology: theory – galaxies : kinematics and dynamics – galaxies: Local Group

## 1. Introduction

Estimating the total masses of galaxies, our own in particular, is a continuing challenge of precision cosmology. Part of the challenge lies in the unknown extent of the dark matter halos within which they are presumably embedded: While the measurement of galaxy rotation curves from coherent stellar motions allows the mass within the visible radius to be inferred, the total mass of the associated dark matter halos predicted in the standard model of cosmology, whose physical extent is not known, is more difficult to estimate. To probe the total effective gravitational mass the analysis must include the effect on the peculiar motions of nearby galaxies.

The measurement of total galaxy masses from their relative motions was pioneered by Kahn & Woltjer 1959. Their “timing argument” (TA) method, which assumes purely radial infall, indicated a total mass for the MW+M31 system of about  $3 \times 10^{12} M_{\odot}$ —a lower bound, since the possibility of transverse motions is excluded. The total mass of the Local Group (LG) can also be computed from the velocity dispersion of its various member galaxies, assuming that it is in virial equilibrium and that its velocity ellipsoid is isotropic: Corteau & Van den Bergh 1999, using this method, found a LG mass of  $(2.3 \pm 0.6) \times 10^{12} M_{\odot}$ . More recent applications of the TA tend to suggest higher masses. Li & White 2008 confirmed that the TA method used on mock galaxies drawn from the Millennium Run (Springel *et al.* 2005) systematically underestimates the true mass, and revised the TA method to predict a LG mass of  $(5.27 \pm 0.5) \times 10^{12} M_{\odot}$ . Van der Marel *et al.* 2012 used the full proper motion of M31 to improve the TA method, estimating a LG mass of about  $5 \times 10^{12} M_{\odot}$ , somewhat higher than the combined prediction of  $(3.17 \pm 0.57) \times 10^{12} M_{\odot}$  from a Bayesian combination of estimates from different methods. The TA can also be used with the proper motion of Leo I (Sohn *et al.* 2012), assuming it is gravitationally bound to the MW, to estimate the mass of the MW alone. Boylan-Kolchin *et al.* 2012 combine the TA and other methods in

estimating a virial mass for the MW of  $1.6 \times 10^{12} M_{\odot}$  with a 90% confidence interval of  $[1.0 - 2.4] \times 10^{12} M_{\odot}$ .

Mass estimation methods using the TA are based on the analysis of single-galaxy interactions with the Milky Way. We show in this paper that the Numerical Action Method (NAM), by taking into account the peculiar motions of a large subset of Local Group satellites, effectively breaks the mass degeneracy in the two-body TA and identifies separate ranges of likely masses for the two principal actors in the LG. The method avoids the TA assumption that galaxies are gravitationally bound, makes no assumptions about virialization of the LG, and is sensitive to more widely diffused concentrations of dark matter that could remain undetected using other methods. NAM takes as input the cosmological parameters  $H_0$  and  $\Omega_0$ , and assumes that linear theory correctly describes velocities at early times and that galaxies and their progenitors back in time can be approximated as simple paths representing the center-of-mass motions of their associated dark matter halos.

Earlier papers on NAM (including Peebles 1989 introducing the method; Peebles 1995; Peebles, *et al.* 2001; Phelps 2002; Peebles, *et al.* 2011; Peebles & Tully 2013) developed the method in the context of the Local Group, focusing on the analysis of individual solutions or small ensembles. In what follows we explore the behavior of several thousand independent solutions in order to identify the combinations of MW and M31 masses that yield the best fit to the observational constraints. Section 1 introduces our implementation of NAM. In section 2 we apply it to the Local Group, and in section 3 we test NAM predictions in the LG with mock catalogs drawn from the Millennium Run. A brief discussion including an assessment of future prospects is found in section 4.

## 2. The numerical action method

### 2.1. Method and approximations

Our version of NAM is based on the improved algorithm described in Peebles *et al.* 2011. We have extended it to include an optional partial canonical transformation of coordinates between the radial distance and the radial velocity (first used in Peebles *et al.* 2001 and more fully described in Phelps 2002), allowing either the galaxy distance or redshift to be chosen as the boundary condition in the action integration at  $z = 0$ , in addition to the two components of the observed galaxy position in the plane of the sky. This effectively doubles the solution space that can be explored. Appendix A gives details of the coordinate transformation.

We model galaxies as constant-density spheres with MW radius of 100 kpc and all other galaxy radii scaling proportionately with the cube root of their masses. From the start of the computation time at  $a = .1$  until  $a = 1$ , galaxy paths are interpreted as the mean motions of the coalescing systems of baryonic matter and their associated dark matter halos. As shown in Peebles *et al.* 2011, the initial velocities are by construction consistent with linear perturbation theory. This keeps the galaxies well separated from each other at early times, and so passages of galaxies through each other’s (nonphysical) cutoff radii are rare.

Galaxy flight paths are reconstructed from initial randomized straight line trial orbits by successive iterations in the direction of the first and second derivatives of the action until a stationary point is reached. Solutions are verified by comparing them to the solutions to the equations of motion from the same initial timestep in a leapfrog approximation. With a target of  $10^{-11}$  in the sum of squares of the gradient of the action, deviations between NAM-generated flight paths and the leapfrog approximation are at most a few kpc at the

final timestep. In the present work we follow Peebles & Tully 2013 in excluding several close satellites to the MW, but we use a smaller number of time steps (30, vs. 500 in Peebles *et al.* 2011 and Peebles & Tully 2013), which is still sufficient to produce tightly bending half-orbits. This significantly reduces computation time and maximizes the number of solutions generated.

NAM solutions are non-unique owing to the mixed boundary conditions: velocities are constrained at the initial time (see discussion in Appendix A, 1.4), while some combination of distances and velocities are fixed at the final time. As a consequence, different choices of initial trial orbits with the same observational constraints will in general yield a different set of galaxy paths, each of which are solutions to the equations of motion. However, as there are more constraints than those required for a solution (it is sufficient to specify either distances or redshifts), a  $\chi^2$  measure of fit is defined for each observable,

$$\chi^2 = \sum_i \left( \frac{model_i - cat_i}{\sigma_i} \right)^2 \quad (1)$$

from which a best-fit solution can be selected from an ensemble.

Apart from the initial trial orbits, solutions may also be sensitive functions of the input parameters (distance, redshift, angular position, and mass), particularly for galaxies in close proximity to each other. These parameters are fixed in the formal NAM computation even though there is an observational uncertainty associated with each. Since we wish to explore the widest possible range of reasonable physical configurations, we adopt the method, similar to Peebles *et al.* 2011 and Peebles & Tully 2013, of defining a  $\chi^2$  measure as a sum over all constraints, fixing the observational constraints as their given values plus a random error within the observational uncertainty:

$$\chi_{tot}^2 = \sum_i (\chi_{i,d}^2 + \chi_{i,cz}^2 + \chi_{i,\theta}^2 + \chi_{i,\phi}^2 + \chi_{i,mass}^2 + \chi_{i,v0}^2) \quad (2)$$

We relax the initial trial orbits to a solution to the equations of motion using NAM, and then relax each NAM solution to a minimum in  $\chi^2$ . By holding some of the observational

constraints relatively fixed, we can repeat this procedure for a large number of NAM solutions to explore an  $n$ -dimensional space of solutions whose minimum in  $\chi^2$  gives the most likely values of the desired  $n$  constraints. In our case we are interested in the masses of the principal actors in the Local Group and so we are looking for a minimum within the two-dimensional space defined by the masses of MW and M31. Further details of our minimization approach, which is fully general and can be applied to any desired combination of observational parameters, are as follows.

For each solution we assign masses to MW and M31 within a range of .5 and  $6 \times 10^{12} M_{\odot}$  in a Gaussian random distribution centered around the nominal masses given in the catalog. This produces higher quality solutions by focusing less attention on combinations of masses which experience has shown are less likely to yield good fits to the constraints. Random errors are added to all other observables (distances, redshifts, angular positions, and masses), with standard deviations taken generically to be 10% of the distance for distances,  $5 \text{ km s}^{-1}$  for redshifts, half a degree for angular positions (allowing the observed galaxies to be offset from the center of mass of their respective halos), and 60% of the nominal catalog masses (giving these quantities the widest possible latitude). Since the main objective of this study is investigating the masses of MW and M31, and good agreement with M31 constraints is therefore a priority, standard deviations in distances, redshifts, and positions for galaxies beyond 1.5 Mpc are doubled and those for M31 are halved. Standard deviations in MW and M31 masses are reduced by a factor of 20 relative to their initial randomized guesses, essentially fixing them in the  $\chi^2$  relaxation step but allowing them to shift by a small amount if a significantly better solution is found at a slightly different mass. As large initial velocities are permitted in the solutions (see Appendix A, 1.4), a contribution to  $\chi^2$  from the magnitude of the initial velocity is additionally assigned with a standard deviation of  $40 \text{ km s}^{-1}$ . This effectively suppresses implausibly large initial velocities in the search for the best solutions.

We find that NAM solutions are efficiently generated by generating a solution for the two dominant galaxies first and then adding the other galaxies, one at a time, in descending order of mass. With each NAM solution we then take each galaxy in turn in the same order, using Powell’s method to relax the individual galaxy distance, redshift and angular position to a minimum in its  $\chi^2$  since derivatives in  $\chi^2$  with respect to these quantities cannot be reliably computed. Discontinuities in  $\chi^2$  may be encountered where a galaxy jumps to a qualitatively different orbit in the descent to the target in the action; these are allowed so long as it leads to an improvement in  $\chi^2$ . If after relaxing with Powell’s method  $\chi^2$  remains above a given threshold (100 yielded a good balance between time to solution and quality of solution), we recast the orbit for this galaxy and find another solution. If, after 50 attempts,  $\chi^2$  is still above the threshold, we switch from distance to redshift boundary conditions for this galaxy and allow another 25 attempts. If  $\chi^2$  still remains above the threshold, we take the solution corresponding to the the lowest  $\chi^2$  found thus far and move to the next galaxy. In practice between 25-50% of the galaxies in any given NAM solution will have been fitted to the velocity boundary condition and the rest to the distance boundary condition. Once  $\chi^2$  has been minimized in this way, we then jointly relax the galaxy masses, also using Powell’s method, to minimize  $\chi^2$  still further (we found that relaxing the masses separately from the other quantities gave more rapid convergence to a minimum). This method of relaxation between the various observational quantities typically reduces  $\chi^2$  by an order of magnitude from its initial value; further improvements to this ad hoc procedure are no doubt possible.

We generate four thousand independent solutions using this method, varying the mass of MW and M31 in each solution as described above. Parallelizing the code to run on 12 supercomputing nodes using 2.40 GHz six-core Xeon processors, each solution typically takes 10 or 20 seconds for catalogs up to a dozen or two particles. From an ensemble of solutions we then plot a gaussian-smoothed  $\chi^2$  map against the MW and M31 masses,



dividing the map into  $24 \times 24$  equal bins and keeping the best  $\chi^2$  in each bin. The smoothing is desirable because the solution space can feature many local minima, each corresponding to a qualitatively different configurations of orbits.

### 3. Results for the Local Group

Our Local Group catalog, based on Peebles & Tully 2013, is listed in Table 1. The omission of tightly bound satellites of MW and M31 facilitates direct comparison to the simulations, which lack comparable dynamic range, and maximizes the number of solutions which can be explored. The four actors listed immediately after MW and M31 are intended to approximately model the influence of the significant mass concentrations residing immediately beyond the Local Group. While inclusion of all Local Group actors may hold the promise of producing even better dynamical constraints on the mass of MW and M31, it is offset by the greatly increased effort required to produce acceptable solutions.

$\chi^2$  maps for 4000 solutions in four different scenarios, all with  $H_0 = 67$  and  $\Omega_0 = .27$ , are shown in Figure 1. At upper left are the contours in  $\chi^2$  generated from a simplified catalog consisting of only MW and M31, to check the consistency of our implementation of NAM with the TA. As expected from the classic TA, we find a well-defined constraint on the sum  $m_{MW} + m_{M31}$  but are unable to resolve the individual masses. The bare TA sum indicated by NAM,  $(m_{LG} = 6 \pm 1) \times 10^{12} M_\odot$  at 95% confidence, is consistent with Li and White (2008), who calibrated the TA against galaxy pairs drawn from the Millennium simulation to find, at 95% confidence,  $1.9 \times 10^{12} M_\odot < M_{LG} < 1.0 \times 10^{13} M_\odot$ , with a median likelihood estimate of  $5.7 \times 10^{12} M_\odot$  (the confidence interval in the latter is larger since it takes cosmic variance into account).

In Figure 1, upper right, we show the results from a reduced version of our catalog

which includes the LG actors but excludes the four external groups. The additional of the additional dynamical actors has broken the degeneracy in the TA, giving independent masses of  $2.5 \pm 1.5 \times 10^{12} M_{\odot}$  for the MW and  $3.5 \pm 1.0 \times 10^{12} M_{\odot}$  for M31. With the addition of the four external groups (Figure 1, lower left), the confidence intervals are broadened and the best mass for the MW increases to  $3.5 \pm 1.5 \times 10^{12} M_{\odot}$ . This is consistent at the upper end with previous TA measurements of the total LG mass and the individual MW mass (as mentioned in the introduction). The result at lower right, which also uses the full catalog but with initial assignment of external masses of 70% that of the result at lower left, shows the robustness of the minimum and suggests a correlation between the additional of external mass and the broadening of the confidence intervals.

#### 4. A test of NAM mass predictions in simulations

As a check on the result for the Local Group, we use publicly available data from the Millennium Run (Springel *et al.* 2005) and follow Li & White 2008 in generating mock Local Group catalogs satisfying the following conditions: We select type 0 or 1 galaxies with rotation velocities in the range  $200 < V_{max} < 250 \text{ km s}^{-1}$  and bulge-to-total luminosity ratio in the range  $1.2 - 2.5$ . We then sub-select close pairs with comoving separation between 0.5 and 1 Mpc, negative relative peculiar velocity and no massive companion with  $V_{max} > 150 \text{ km s}^{-1}$  within 2.5 Mpc from the centre-of-mass. This led to the initial identification of about 100 Local Group candidates. Since the simulation overproduces satellite galaxies relative to observations (the “missing satellite problem”; see e.g. Bullock 2012), and since the resulting dynamical complexity poses a special difficulty for NAM reconstructions, we additionally exclude catalogs where the gravitational acceleration on mock-MW due to satellites is greater by more than a factor of six than what we expect from the observed distribution (assuming the distance and nominal masses listed in our

catalog). This limited our set of mock catalogs to 32 with reasonably similar dynamics to what expect to be the case with the LG, although in every case but two the dynamical complexity as defined above is greater than in the LG. To speed up computation time, within each of the 32 selected mock catalogs we include in the NAM computation only those galaxies and satellites within the distance to mock-M31, and all other galaxies out to 7 Mpc which produce an acceleration of at least 5% that of M31. This reduced the number of particles to those that are most relevant to the dynamics of the principal actors – from as few as 9 to as many as 34, with an average across the catalogs of 19.

Contours in  $\chi^2$  for different halo masses of mock-MW and mock-M31 are shown for the four dynamically simplest catalogs in Figure 2. The predicted values for their masses are consistent with the true galaxy + halo masses from the simulation, within the 95% confidence range. We may expect the NAM prediction to be somewhat higher if it is sensitive to dark matter associated with the two principal actors but beyond their respective cutoff radii (at an overdensity of 200) that define their masses. A detailed comparison of the underlying dark matter distribution with the halo mass predictions may indicate whether this sensitivity is present. For the other 28 mock catalogs the mass predictions for both actors were likewise consistent with the 95% confidence intervals in all but three cases. The NAM-based mass predictions from the mock catalogs are thus accurate within statistical expectations.

## 5. Discussion

We have shown that the Numerical Action Method offers a promising method of constraining individual masses of the principal actors in the Local Group using an approach that investigates the behavior of  $\chi^2$  across a large ensemble of solutions. It is complementary to earlier work focusing on the detailed dynamical analysis of individual solutions.

The relatively large masses of MW and M31 suggested in this first-of-its-kind implementation of NAM are a point of interest. They may be due to the method’s sensitivity to both the extended dark matter halo as well as purely dark concentrations between galaxies, since these otherwise invisible concentrations should leave a signature in galaxy proper motions. Another possibility is that the result is biased by poor reconstruction of satellite paths, since solutions placing M31 at exactly the observed distance and redshift also tend to place the dwarf galaxies in the near vicinity of the MW at distances much greater than the catalog distance.

We note, as well, that tangential velocities of M31 are a sensitive function of the presence of external groups: in the absence of the former  $v_{tan,M31}$  are typically less than  $50 \text{ km s}^{-1}$ , while with external masses  $v_{tan,M31}$  are typically  $100 \text{ km s}^{-1}$  or more. Recent observational constraints on  $v_{tan,M31}$  by Van der Marel *et al.* (2012) indicate  $v_{tan,M31} \leq 34.3 \text{ km s}^{-1}$  at  $1\sigma$  confidence. If a tangential velocity constraint for selected galaxies such as M31 were added to  $\chi^2$ , and if further work on the observational side confirms a low  $v_{tan,M31}$ , this could place significant additional constraints on the solution space.

Further improvements to this method are suggested by the above observations, and can be expected from a number of directions. On the computational side, increases in the efficiency of the solution finding algorithm will permit a larger number of time steps to be used and potentially allow for more complex orbits, improving in particular the reconstruction of nearby satellites. It will also permit a larger complement of dwarf and satellite galaxies to be included. Adding full three-dimensional proper motions of nearby galaxies will certainly further constrain the likely masses. A comparison of the underlying dark matter distribution with the galaxy halos in the simulations will confirm whether NAM is potentially sensitive to extended distributions of dark matter beyond the nominal

halo radii.

## 6. Appendix: A faster NAM in redshift space

Sections 1 and 2 are from Peebles *et al.* 2011. Section 3 is new to this study and shows how the action can be modified to accommodate redshift boundary conditions.

### 1. Review of the theory

#### 1.1. Equations of motion

In a cosmologically flat universe the expansion parameter satisfies

$$\frac{\dot{a}^2}{a^2} = \frac{H_o^2 \Omega}{a^3} + (1 - \Omega)H_o^2, \quad \frac{\ddot{a}}{a} = -\frac{H_o^2 \Omega}{2a^3} + (1 - \Omega)H_o^2, \quad (3)$$

with present value  $a_o = 1$ . The equations of motion in physical length units are

$$\frac{d^2 r_{i,k}}{dt^2} = \sum_{j \neq i} \frac{Gm_j(r_{j,k} - r_{i,k})}{|r_i - r_j|^3} + (1 - \Omega)H_o^2 r_{i,k}. \quad (4)$$

Changing variables to the comoving coordinates  $x_{i,k} = r_{i,k}/a(t)$  used here brings eq. (4) to

$$\frac{d}{dt} a^2 \frac{dx_{i,k}}{dt} = \frac{1}{a} \left[ \sum_j Gm_j \frac{(x_{j,k} - x_{i,k})}{|x_i - x_j|^3} + \frac{1}{2} \Omega H_o^2 x_{i,k} \right]. \quad (5)$$

This is derived from the action

$$S = \int_0^{t_o} dt \left[ \sum_i \frac{m_i a^2 \dot{x}_i^2}{2} + \frac{1}{a} \left( \sum_{j \neq i} \frac{Gm_i m_j}{|x_i - x_j|} + \frac{1}{4} \sum_i m_i \Omega H_o^2 x_i^2 \right) \right] \quad (6)$$

when the present positions are fixed,  $\delta x_i(t_o) = 0$ , and initial conditions satisfy

$$a^2 \dot{x}_i \rightarrow 0 \text{ at } a(t) \rightarrow 0. \quad (7)$$

#### 1.2. Discrete representation

In a discrete representation the coordinates are  $x_{i,k,n}$ , where  $i$  labels the particles,  $k = 1, 2, 3$  the Cartesian coordinates, and  $1 \leq n \leq n_x + 1$  the time steps. The present positions  $x_{i,k,n_x+1}$  are fixed and given. The relevant derivatives of the action are

$$S_{i,k,n} = \frac{\partial S}{\partial x_{i,k,n}}, \quad S_{i,k,n;j,k',n'} = \frac{\partial^2 S}{\partial x_{i,k,n} \partial x_{j,k',n'}}, \quad 1 \leq n, n' \leq n_x. \quad (8)$$

If  $S$  is close to quadratic in the  $x_{i,k,n}$  then position shifts  $\delta x_{i,k,n}$  to a solution at an extremum of  $S$  satisfy

$$S_{i,k,n} + \sum_{j,k',n'} S_{i,k,n;j,k',n'} \delta x_{j,k',n'} = 0. \quad (9)$$

If the  $x_{i,k,n}$  are not close to a solution  $S$  is not close to quadratic in the  $x_{i,k,n}$ , but experience shows that coordinate shifts in the direction of  $\delta x_{i,k,n}$  walk toward a solution.

Approximate the action (4) as

$$\begin{aligned} S = & \sum_{i,k,n=1,n_x} \frac{m_i}{2} \frac{(x_{i,k,n+1} - x_{i,k,n})^2}{(a_{n+1} - a_n)} \dot{a}_{n+1/2} a_{n+1/2}^2 \\ & + \sum_{i,j,n=1,n_x} \frac{t_{n+1/2} - t_{n-1/2}}{a_n} \left[ \sum_{j < i} \frac{G m_i m_j}{|x_{i,n} - x_{j,n}|} + \frac{1}{4} \sum_i m_i \Omega H_o^2 x_{i,n}^2 \right]. \end{aligned} \quad (10)$$

The times  $t_{n\pm 1/2}$  interpolate between the time steps at  $n$  and  $n \pm 1$  in leapfrog fashion. The approximation to the kinetic energy in eq. (10) is motivated by linear perturbation theory, where  $dx/da$  is nearly independent of time, so  $(x_{n+1} - x_n)/(a_{n+1} - a_n)$  is a good approximation to  $dx/da$  at  $a_{n+1/2}$ . The earliest time at which positions are computed is at  $a_1 > 0$ . The leapfrog back in time from  $a_1$  is to  $a_{1/2} = 0 = t_{1/2}$ . Recall that present positions at  $a_{n_x+1} = 1$  are given at  $x_{i,k,n_x+1}$ .

The derivative of the action with respect to the coordinates  $x_{i,k,n}$  for  $1 \leq n \leq n_x$ , gives

$$\begin{aligned} S_{i,k,n} = & -\frac{a_{n+1/2}^2 \dot{a}_{n+1/2}}{a_{n+1} - a_n} (x_{i,k,n+1} - x_{i,k,n}) \\ & + \frac{t_{n+1/2} - t_{n-1/2}}{a_n} \left[ \sum_{j \neq i} G m_j \frac{x_{j,k,n} - x_{i,k,n}}{|x_{i,n} - x_{j,n}|^3} + \frac{1}{2} \Omega H_o^2 x_{i,k,n} \right] \\ & + \frac{a_{n-1/2}^2 \dot{a}_{n-1/2}}{a_n - a_{n-1}} (x_{i,k,n} - x_{i,k,n-1}). \end{aligned} \quad (11)$$

When  $S_{i,k,n} = 0$  this is a discrete approximation to the equation of motion (5). The common factor  $m_i$  has been dropped to reduce clutter, which means  $S_{i,k,n;j,k',n'} \neq S_{j,k',n';i,k,n}$ . (The asymmetry is in the gravity term. There still is the symmetry  $S_{i,k,n;i,k',n'} = S_{i,k',n';i,k,n}$ .)

To simplify eq. (11) and its derivatives wrt  $x_{i,k,n}$  let

$$F_n^+ = \frac{a_{n+1/2}^2 \dot{a}_{n+1/2}}{a_{n+1} - a_n}, \quad F_n^- = \frac{a_{n-1/2}^2 \dot{a}_{n-1/2}}{a_n - a_{n-1}} = F_{n-1}^+, \quad \frac{dt_n}{a_n} = \frac{t_{n+1/2} - t_{n-1/2}}{a_n}. \quad (12)$$

Note that

$$F_1^- = 0 = F_0^+ \quad (13)$$

follows from  $a^2 \dot{a} \rightarrow 0$  at  $a \rightarrow 0$ . Also, write the acceleration (apart from the factor  $a^2$ ) of particle  $i$  due to the other particles  $j \neq i$  as

$$g_{i,k,n} = \sum_{j \neq i} Gm_j \frac{x_{j,k,n} - x_{i,k,n}}{|x_{i,n} - x_{j,n}|^3}. \quad (14)$$

All this notation brings eq. (11) to

$$S_{i,k,n} = -F_n^+(x_{i,k,n+1} - x_{i,k,n}) + F_n^-(x_{i,k,n} - x_{i,k,n-1}) + \frac{dt_n}{a_n} \left[ g_{i,k,n} + \frac{1}{2} \Omega H_o^2 x_{i,k,n} \right]. \quad (15)$$

We need the derivatives of the action with respect to the positions of the particles. Let the derivative of the acceleration of particle  $i$  wrt the position of particle  $j \neq i$  be

$$\begin{aligned} \mathcal{G}_{i,k,n;j,k'} &= \frac{\partial g_{i,k,n}}{\partial x_{j,k',n}} \\ &= Gm_j \left( \frac{\delta_{k,k'}}{|x_{i,n} - x_{j,n}|^3} - 3 \frac{(x_{j,k,n} - x_{i,k,n})(x_{j,k',n} - x_{i,k',n})}{|x_{i,n} - x_{j,n}|^5} \right). \end{aligned} \quad (16)$$

The derivative of the acceleration of particle  $i$  with respect to its own position is

$$\mathcal{G}_{i,k,n;i,k'} = \frac{\partial g_{i,k,n}}{\partial x_{i,k',n}} = - \sum_{j \neq i} \mathcal{G}_{i,k,n;j,k'} \quad (17)$$

So the nonzero derivatives of eq. (15) with respect to the coordinates are

$$\begin{aligned} S_{i,k,n;i,k,n+1} &= -F_n^+, & S_{i,k,n;i,k,n-1} &= -F_n^-, \\ S_{i,k,n;j,k',n} &= \frac{dt_n}{a_n} \mathcal{G}_{i,k,n;j,k'}, \quad j \neq i, \\ S_{i,k,n;i,k',n} &= (F_n^+ + F_n^-) \delta_{k,k'} + \frac{dt_n}{a_n} \left[ \mathcal{G}_{i,k,n;i,k'} + \frac{1}{2} \Omega H_o^2 \delta_{k,k'} \right]. \end{aligned} \quad (18)$$

The goal is to use these second derivatives of the action to drive the first derivatives to zero at a stationary point,  $S_{i,k,n} = 0$ .

### 1.3. Leapfrog integration forward in time

It is worth recording that when the action is at a stationary point,  $S_{i,k,n} = 0$ , a solution of equation (15) is equivalent to a standard leapfrog numerical integration of the equation of motion (5) forward in time. In this leapfrog, the positions and velocities are computed at interleaved time steps as (in the notation in eq [12]),

$$a_{n+1/2}^2 \dot{x}_{i,k,n+1/2} = a_{n-1/2}^2 \dot{x}_{i,k,n-1/2} + \frac{dt_n}{a_n} \left[ \sum_{j \neq i} g_{i,k,n;j} + \frac{1}{2} \Omega H_o^2 x_{i,k,n} \right], \quad (19)$$

and

$$x_{i,k,n+1} = x_{i,k,n} + \dot{x}_{i,k,n+1/2}(t_{n+1} - t_n) = x_{i,k,n} + \dot{x}_{i,k,n+1/2}(a_{n+1} - a_n)/\dot{a}_{n+1/2}, \quad (20)$$

which in the notation in eq (12) is

$$x_{i,k,n+1} = x_{i,k,n} + a_{n+1/2}^2 \dot{x}_{i,k,n+1/2} / F_n^+. \quad (21)$$

Equations (19) and (21) are equivalent to eq. (15) at  $S_{i,k,n} = 0$ .

The difference from a conventional leapfrog integration is the boundary conditions, which here are the present positions and a condition on the initial velocities, as follows.

### 1.4. Initial conditions

The representation of the mass distribution in the early universe by galaxy-size particles certainly is crude, but a reasonably useful approximation that motivates the following consideration.

In linear perturbation theory for a continuous pressureless fluid the unwanted decaying mode has peculiar velocity that is decreasing as  $v = a\dot{x} \propto 1/a(t)$ . Eq. (7) formally



eliminates this decaying mode. In the wanted growing mode the coordinate position of a particle is changing with time as

$$x(t) - x(0) \propto t^{2/3} \propto a(t). \quad (22)$$

This implies that in the wanted growing mode the left hand side of eq. (5) is constant, meaning  $a^2 dx_{i,k}/dt \simeq \text{constant} \times t$ , where  $t$  is the time measured from  $a = 0$ . This motivates approximating equation (5) at the time  $t_{3/2}$  intermediate between the first two time steps in the leapfrog,  $a_1$  and  $a_2$ , as

$$a_{3/2}^2 \frac{dx_{i,k,3/2}}{dt} \simeq a_{3/2}^2 \dot{a}_{3/2} \frac{x_{i,k,2} - x_{i,k,1}}{a_2 - a_1} = \frac{t_{3/2}}{a_1} \left[ \sum_j Gm_j \frac{(x_{j,k,1} - x_{i,k,1})}{|x_i - x_j|^3} + \frac{1}{2} \Omega H_o^2 x_{i,k,1} \right], \quad (23)$$

Recall that the half time step earlier than  $a_1$  is at  $a_{1/2} = 0 = t_{1/2} = 0$ , where  $a^2 \dot{x}$  is supposed to vanish. Equation (23) agrees with equations (13) and (15) at  $S_{i,k,1} = 0$ .

It will be noted that  $a_1$  may be much larger than  $a_2 - a_1$ , meaning the numerical solution commences at modest redshift with small time steps. But  $t_{3/2}$  is still the time from  $a_{1/2} = 0$  to the time midway between  $a_1$  and  $a_2$ .

The prescription in eq. (23) allows large peculiar velocities at high redshift. This is not inconsistent with eq. (7); it corresponds to a large primeval departure from homogeneity. It does mean that one must select solutions that are judged to have realistic initial peculiar velocities (at  $a_{3/2}$ ).

To summarize, the usual initial conditions — position and velocity — in a leapfrog integration of the equation of motion forward in time are replaced by the present position,  $x_{i,k,n_x+1}$ , and the relation in equation (23) between the two earliest positions,  $x_{i,k,1}$  and  $x_{i,k,2}$ , at times  $t_1$  and  $t_2$ . If equation (22) is a good approximation this is equivalent to specifying the initial velocity, for then eq. (23) determines  $\dot{x}_{3/2}$ . That is, the boundary conditions for a solution  $S_{i,k,n} = 0$  are the present position and the time-variation of the initial velocity.

## 2. Method of solution

### 2.1. Single orbit adjustment

Since we're adjusting only the orbit of particle  $i$  drop the label  $i$  and write the first derivative of  $S$  as

$$\frac{\partial S}{\partial x_{k,n}} = S_{k,n} = -F_n^+(x_{k,n+1} - x_{k,n}) + F_n^-(x_{k,n} - x_{k,n-1}) + \frac{dt_n}{a_n} \left( \sum_{j \neq i} g_{k,n;j} + \frac{\Omega H_o^2}{2} x_{k,n} \right), \quad (24)$$

and write the equation to be solved as

$$S_{k,n} + \sum_{k',n'} S_{k,n;k',n'} \delta x_{k',n'} = 0, \quad \frac{\partial^2 S}{\partial x_{k,n} \partial x_{k',n'}} = S_{k,n;k',n'} = S_{k',n';k,n}. \quad (25)$$

The nonzero second derivatives are

$$S_{k,n;k,n+1} = -F_n^+, \quad (26)$$

$$S_{k,n;k',n} = (F_n^+ + F_n^-) \delta_{k,k'} + \frac{dt_n}{a_n} \left( \sum_{j \neq i} \mathcal{G}_{k,n;jk'} + \frac{\Omega H_o^2}{2} \delta_{k,k'} \right). \quad (27)$$

Since

$$S_{k,n;k',n'} = 0 \text{ unless } n' = n \text{ or else } n' = n \pm 1 \text{ and } k' = k, \quad (28)$$

eq. (25) is

$$S_{k,n} + S_{k,n;k,n+1} \delta x_{k,n+1} + \sum_{k'} S_{k,n;k',n} \delta x_{k',n} + S_{k,n;k,n-1} \delta x_{k,n-1} = 0. \quad (29)$$

Set  $n \rightarrow n-1$  in this equation and rearrange it to

$$\delta x_{k,n} = - \frac{S_{k,n-1} + \sum_{k'} S_{k,n-1;k',n-1} \delta x_{k',n-1} + S_{k,n-1;k,n-2} \delta x_{k,n-2}}{S_{k,n-1;k,n}}. \quad (30)$$

This gives  $\delta x_{k,n}$  in terms of  $\delta x_{k,n-1}$  and  $\delta x_{k,n-2}$ . On iterating we get the form

$$\delta x_{k,n} = A_{k,n} + \sum_{k''} B_{k,n;k''} \delta x_{k'',1}. \quad (31)$$

At  $n=1$  this is just

$$A_{k,1} = 0, \quad B_{k,1;k''} = \delta_{k,k''}. \quad (32)$$

At the second time step from the start,  $n = 2$ , eq. (30) is

$$\delta x_{k,2} = - \left[ S_{k,1} + \sum_{k'} S_{k,1;k',1} \delta x_{k',1} \right] / S_{k,1;k,2}, \quad (33)$$

because there is no  $\delta x_{k,0}$ . Comparing this with eq. (31) we see that

$$A_{k,2} = -S_{k,1}/S_{k,1;k,2}, \quad B_{k,2;k'} = -S_{k,1;k',1}/S_{k,1;k,2}. \quad (34)$$

At  $n \geq 3$  the result of substituting the form (31) into eq. (30) is

$$\begin{aligned} \delta x_{k,n} = & - \left[ S_{k,n-1} + \sum_{k'} S_{k,n-1;k',n-1} (A_{k',n-1} + \sum_{k''} B_{k',n-1;k'',1} \delta x_{k'',1}) \right. \\ & \left. + S_{k,n-1;k,n-2} (A_{k,n-2} + \sum_{k''} B_{k,n-2;k'',1} \delta x_{k'',1}) \right] / S_{k,n-1;k,n}. \end{aligned} \quad (35)$$

So at  $3 \leq n \leq n_x$

$$\begin{aligned} A_{k,n} &= - \frac{S_{k,n-1} + \sum_{k'} S_{k,n-1;k',n-1} A_{k',n-1} + S_{k,n-1;k,n-2} A_{k,n-2}}{S_{k,n-1;k,n}}, \\ B_{k,n;k''} &= - \frac{\sum_{k'} S_{k,n-1;k',n-1} B_{k',n-1;k'',1} + S_{k,n-1;k,n-2} B_{k,n-2;k'',1}}{S_{k,n-1;k,n}}. \end{aligned} \quad (36)$$

Eqs (34) and (36) give the  $A_{k,n}$  and  $B_{k,n;k''}$ ,  $2 \leq n \leq n_x$ , in terms of the input derivatives of the action. Then eq. (31) is  $3n_x - 3$  equations for the  $\delta x_{k,n}$ , at  $2 \leq n \leq n_x$ , in terms of the  $\delta x_{k,1}$ . We get three more, which fix the  $\delta x_{k,1}$ , by setting  $n = n_x$  in equation (29) and recalling that  $\delta x_{k,n_x+1} = 0$ :

$$\begin{aligned} 0 &= S_{k,n_x} + \sum_{k'} S_{k,n_x;k',n_x} \delta x_{k',n_x} + S_{k,n_x;k,n_x-1} \delta x_{k,n_x-1} \\ &= S_{k,n_x} + \sum_{k'} S_{k,n_x;k',n_x} \left[ A_{k',n_x} + \sum_{k''} B_{k',n_x;k'',1} \delta x_{k'',1} \right] \\ &\quad + S_{k,n_x;k,n_x-1} \left[ A_{k,n_x-1} + \sum_{k''} B_{k,n_x-1;k'',1} \delta x_{k'',1} \right]. \end{aligned} \quad (37)$$

So write this as

$$\begin{aligned} 0 &= T_k + \sum_{k'} T_{k,k''} \delta x_{k'',1}, \\ T_k &= S_{k,n_x} + \sum_{k'} S_{k,n_x;k',n_x} A_{k',n_x} + S_{k,n_x;k,n_x-1} A_{k,n_x-1}, \\ T_{k,k''} &= \sum_{k'} S_{k,n_x;k',n_x} B_{k',n_x;k'',1} + S_{k,n_x;k,n_x-1} B_{k,n_x-1;k'',1}, \end{aligned} \quad (38)$$

solve this  $3 \times 3$  set of equations for the  $\delta x_{k,1}$ , and then get the rest of the  $\delta x_{k,n}$  from eq. (31).

### 3. Redshift boundary condition

Solutions to the equations of motion in the method outlined in 2. above satisfy the constraint that the distances at the present epoch are fixed. However, since redshifts are known more accurately than the distances, and since we may want to explore a larger space of solutions, it may be desirable to recast the problem with fixed redshifts, with the distances at the present epoch emerging as predictions. (note that the choice of boundary condition can be made particle-by-particle.) This can be accomplished through a partial transformation of coordinates that exchanges radial distances with radial velocities while leaving the angular position coordinates unchanged. Details are given in Phelps (2002); the procedure is summarized below.

The change to radial velocity coordinates is carried out in the Hamiltonian frame through a canonical transformation of the conjugate variables (positions and momenta). The generating function of the transformation, which is added to the action outside the integral, is

$$- p_{i,r,nx+1} q_{i,r,nx+1}, \quad (39)$$

Where  $q_r$  and  $p_r$  are the conjugate distance and momentum in the radial direction relative to the reference galaxy. With the addition of the generating function, the problem becomes equivalent to one expressed with a new set of conjugate coordinates  $Q_r$  and  $P_r$ , where  $Q_r$  is the radial momentum and  $P_r$  is the radial distance. In these coordinates the boundary term in the variational derivative  $P\delta Q$  vanishes at  $z = 0$  when the *angular* positions and the *radial* velocity vanish. However, since the transformed Hamiltonian cannot be expressed analytically (the gravitational term cannot be written out in terms of  $Q$ ), the computation must be carried out in the original coordinate system, expressed in the Lagrangian frame,

where the new boundary condition must be imposed by hand to recover the correct equations of motion. That constraint takes the form of additional terms in the action, as follows.

### 3.1 Modification to the action

The modified action is:

$$\begin{aligned}
S &= \frac{1}{2} H_0 x_{i,r,nx+1}^2 - cz x_{i,r,nx+1} + x_{i,r,nx+1} \vec{v}_{mw,nx+1} \cdot \hat{r}_{i,nx+1} \\
&+ \sum_{i,k,n=1,n_x} \frac{1}{2} \frac{(x_{i,k,n+1} - x_{i,k,n})^2}{(a_{n+1} - a_n)} \dot{a}_{n+1/2} a_{n+1/2}^2 \\
&+ \sum_{i,j,n=1,n_x} \frac{t_{n+1/2} - t_{n-1/2}}{a_n} \left[ \sum_{j<i} \frac{Gm_j}{|x_{i,n} - x_{j,n}|} + \frac{1}{4} \sum_i \Omega H_o^2 x_{i,n}^2 \right]. \quad (40)
\end{aligned}$$

The gradient at the final time step is:

$$\begin{aligned}
S_{i,k,n} &= H_0 x_{i,r,nx+1} - cz + \vec{v}_{mw,nx+1} \cdot \hat{r}_{i,nx+1} \\
&- F_n^+(x_{i,k,n+1} - x_{i,k,n}) + F_n^-(x_{i,k,n} - x_{i,k,n-1}) + \frac{dt_n}{a_n} \left[ g_{i,k,n} + \frac{1}{2} \Omega H_o^2 x_{i,k,n} \right]. \quad (41)
\end{aligned}$$

The modified second derivatives of the action at the final two timesteps are:

$$S_{i,k,nx;i,k,nx+1} = - \frac{\hat{x}_{i,k,nx+1}}{dt_{nx+1}} \quad (42)$$

Note that a new term in the action  $S_{k,nx+1;k,nx+1}$  is also present, but it is not used in the computation that follows.

Since the boundary condition is now velocity-limited,  $\delta x_{k,nx+1} \neq 0$ , and we must add a new term in eq. (39) arising from the final two timesteps:

$$\begin{aligned}
0 &= S_{k,nx} + \sum_{k'} S_{k,nx;k',nx} \delta x_{k',nx} + S_{k,nx;k,nx-1} \delta x_{k,nx-1} \\
&\quad + S_{k,nx;k,nx+1} \delta x_{k,nx+1} \\
&= S_{k,nx} + \sum_{k'} S_{k,nx;k',nx} \left[ A_{k',nx} + \sum_{k''} B_{k',nx;k''} \delta x_{k'',1} \right]
\end{aligned}$$

$$\begin{aligned}
& + S_{k,n_x;k,n_x-1} \left[ A_{k,n_x-1} + \sum_{k''} B_{k,n_x-1;k''} \delta x_{k'',1} \right] \\
& + S_{k,n_x;k,n_x+1} \left[ A_{k,n_x+1} + \sum_{k''} B_{k,n_x+1;k''} \delta x_{k'',1} \right].
\end{aligned} \tag{43}$$

This is now written as

$$\begin{aligned}
0 &= T_k + \sum_{k'} T_{k,k'} \delta x_{k',1}, \\
T_k &= S_{k,n_x} + \sum_{k'} S_{k,n_x;k',n_x} A_{k',n_x} + S_{k,n_x;k,n_x-1} A_{k,n_x-1}, \\
&+ S_{k,n_x;k,n_x+1} A_{k,n_x+1}, \\
T_{k,k'} &= \sum_{k''} S_{k,n_x;k',n_x} B_{k',n_x;k''} + S_{k,n_x;k,n_x-1} B_{k,n_x-1;k''}, \\
&+ S_{k,n_x;k,n_x+1} B_{k,n_x+1;k''}.
\end{aligned} \tag{44}$$

As before, this  $3 \times 3$  set of equations is solved for the  $\delta x_{k,1}$ , and we get the rest of the  $\delta x_{k,n}$  from eq. (31). However, we will find below that the boundary conditions will enable us to replace the  $\delta x_{n_x+1}$  above with functions of  $\delta x_{n_x}$ .

### 3.2 Modification to the position shifts

The change of boundary conditions implies a relationship between the position shifts  $\delta x_{k,n_x+1}$  and  $\delta x_{k,n_x}$  that will further modify the new terms above. The relationship is simplest to see in the one-dimensional case (setting  $y = z = 0$ ), where

$$\begin{aligned}
cz &= v_{n_x+1} + H_0 x_{n_x+1} - v_{mw,n_x+1}. \\
&= \frac{x_{n_x+1} - a_{n_x} x_{n_x}}{dt_{n_x+1/2}} + H_0 (x_{n_x+1} - x_{mw,n_x+1}) - v_{mw,n_x+1},
\end{aligned} \tag{45}$$

where we continue to drop the particle subscript unless referring to the reference galaxy,  $mw$ , since we are working on one particle at a time while holding the rest of the catalog fixed.

After the variation,

$$cz' = \frac{x_{n_x+1} + \delta x_{n_x+1} - a_{n_x} x_{n_x} - a_{n_x} \delta x_{n_x}}{dt_{n_x+1/2}}$$

$$+H_0(x_{nx+1} + \delta x_{nx+1} - x_{mw,nx+1}) - v_{mw,nx+1}. \quad (46)$$

Recall that the orbit of the reference galaxy, and thus its contribution to the redshift, is held constant during the variation.

Setting  $cz' = cz$  gives

$$\delta x_{nx+1} = \frac{a_{nx}\delta x_{nx}}{1 + H_0 dt_{nx+1/2}}. \quad (47)$$

In three dimensions the angular coordinates of the particle must also remain unchanged after the variation, and so now there are three equations constraining the coordinate shifts at the final two timesteps:

$$cz' = cz, \quad \theta' = \theta, \quad \phi' = \phi, \quad (48)$$

where  $\theta$  and  $\phi$  are defined relative to the reference galaxy at  $z = 0$ :

$$\tan \theta_{nx+1} = \frac{x_{2,nx+1} - x_{mw,2,nx+1}}{x_{1,nx+1} - x_{mw,1,nx+1}} \quad (49)$$

$$\tan \phi_{nx+1} = \frac{x_{3,nx+1} - x_{mw,3,nx+1}}{\sqrt{(x_{1,nx+1} - x_{mw,1,nx+1})^2 + (x_{2,nx+1} - x_{mw,2,nx+1})^2}}. \quad (50)$$

The  $\theta$  and  $\phi$  constraints impose a relationship between the three  $\delta x_{k,nx+1}$ . The  $\theta$  constraint gives:

$$\begin{aligned} \theta'_{nx+1} &= \theta_{nx+1} \\ \frac{x'_2}{x'_1} &= \frac{x_2}{x_1} \\ \frac{x_{2,nx+1} - x_{mw,2,nx+1} + \delta x_{2,nx+1}}{x_{1,nx+1} - x_{mw,1,nx+1} + \delta x_{1,nx+1}} &= \frac{x_{2,nx+1} - x_{mw,2,nx+1}}{x_{1,nx+1} - x_{mw,1,nx+1}} \\ \delta x_{2,nx+1} &= \frac{x_{2,nx+1}}{x_{1,nx+1}} \delta x_{1,nx+1}. \end{aligned} \quad (51)$$

The combined  $\theta$  and  $\phi$  constraints further give:

$$\phi'_{nx+1} = \phi_{nx+1}$$

$$\begin{aligned}\frac{x_1'^2 + x_2'^2}{x_3'^2} &= \frac{x_1^2 + x_2^2}{x_3^2} \\ \delta x_{3,nx+1} &= \frac{x_{3,nx+1}}{x_{1,nx+1}} \delta x_{1,nx+1}.\end{aligned}\tag{52}$$

As for the third constraint, the redshift in three dimensions is:

$$\begin{aligned}cz &= (\vec{v}_{nx+1} - \vec{v}_{mw,nx+1}) \cdot \hat{r}_{nx+1} + H_0 r_{nx+1} \\ &= \sum_k \left( \frac{x_{k,nx+1} - a_{nx} x_{k,nx}}{dt_{nx+1/2}} - \vec{v}_{mw,nx+1} \right) \cdot \hat{x}_{k,nx+1} \\ &\quad + H_0 \sqrt{\sum_k (x_{k,nx+1} - x_{mw,k,nx+1})^2},\end{aligned}\tag{53}$$

where

$$\hat{x}_{k,nx+1} = \frac{x_{k,nx+1}}{r_{nx+1}} = \frac{x_{k,nx+1}}{\sqrt{\sum_{k'} (x_{k',nx+1} - x_{mw,k',nx+1})^2}}.\tag{54}$$

After the position shifts,

$$\begin{aligned}cz' &= \sum_k \left( \frac{x_{k,nx+1} + \delta x_{k,nx+1} - a_{nx} x_{k,nx} - a_{nx} \delta x_{k,nx}}{dt_{nx+1/2}} - \vec{v}_{mw,k,nx+1} \right) \cdot \hat{x}'_{k,nx+1} \\ &\quad + H_0 \sqrt{\sum_k (x_{k,nx+1} - x_{mw,k,nx+1} + \delta x_{k,nx+1})^2}\end{aligned}\tag{55}$$

where

$$\hat{x}'_{k,nx+1} = \frac{x_{k,nx+1} + \delta x_{k,nx+1}}{\sqrt{\sum_{k'} (x_{k',nx+1} - x_{mw,k',nx+1} + \delta x_{k',nx+1})^2}}.\tag{56}$$

Setting  $cz' = cz$  and using the approximation  $\delta x_k/x_k \ll 1$ , we find, after some algebra,

$$\delta x_{k,nx+1} = \frac{x_{k,nx+1}}{\alpha} \sum_{k'} x_{k',nx+1} a_{nx} \delta x_{k',nx},\tag{57}$$

where

$$\alpha = \sum_{k''} x_{k'',nx+1} \left( x_{k'',nx+1} (2 - \beta) - a_{nx} x_{k'',nx} - v_{mw,k'',nx+1} dt_{nx+1/2} \right)\tag{58}$$

$$\beta = 1 - H_0 dt_{nx+1/2} - \sum_{k'''} \frac{x_{k''',nx+1} a_{nx} x_{k''',nx} + x_{k''',nx+1} v_{mw,k''',nx+1} dt_{nx+1/2}}{r_{nx+1}^2}.\tag{59}$$



It can be shown that this reduces to the one-dimensional case when we set two of the three position coordinates to zero.

With the above, the position shifts  $\delta x_{k,nx+1}$  can be replaced in eqs. (43-44) by their equivalent expressions in terms of  $\delta x_{k,nx}$ :

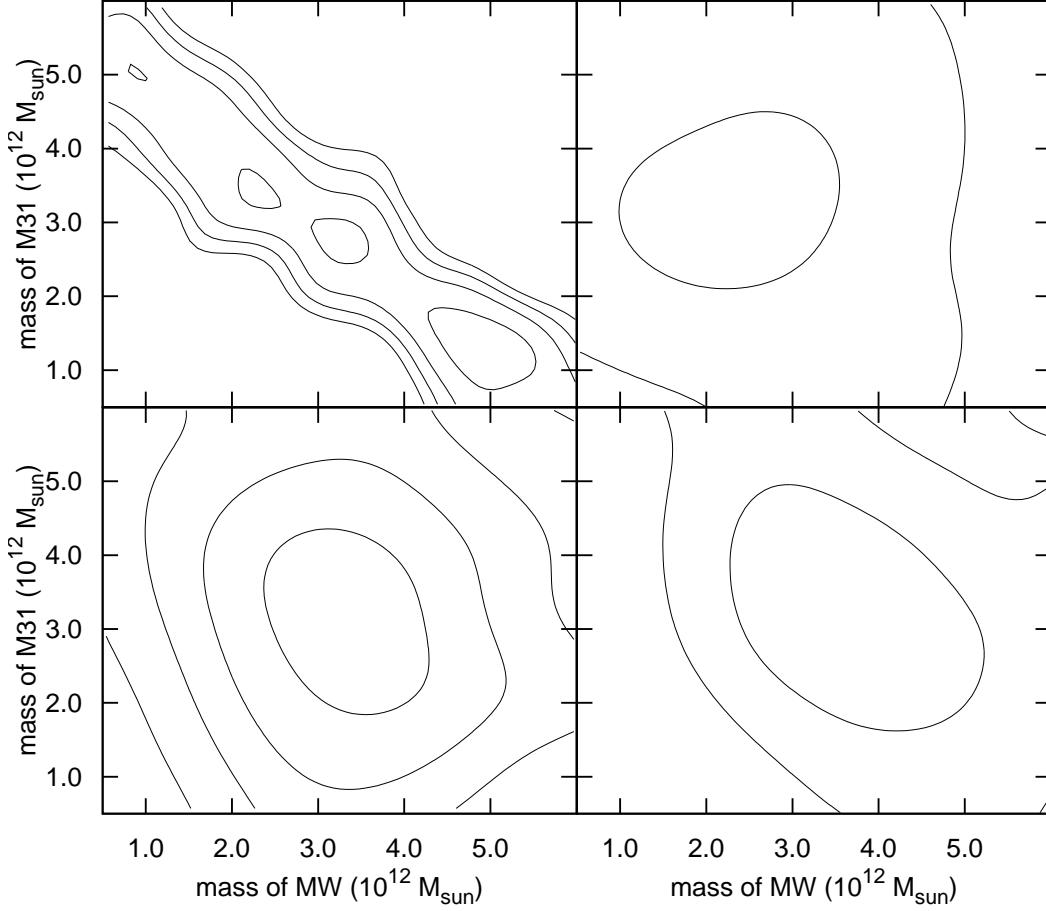
$$\begin{aligned}
0 = & S_{k,nx} + \sum_{k'} S_{k,nx;k',nx} \left[ A_{k',nx} + \sum_{k''} B_{k',nx;k'',1} \delta x_{k'',1} \right] \\
& + S_{k,nx;k,nx-1} \left[ A_{k,nx-1} + \sum_{k''} B_{k,nx-1;k'',1} \delta x_{k'',1} \right] \\
& + S_{k,nx;k,nx+1} x_{k,nx+1} \alpha^{-1} \sum_{k'} x_{k',nx+1} \left[ A_{k',nx} + \sum_{k''} B_{k',nx;k'',1} \delta x_{k'',1} \right].
\end{aligned} \tag{60}$$

$$\begin{aligned}
0 = & T_k + \sum_{k'} T_{k,k''} \delta x_{k'',1}, \\
T_k = & S_{k,nx} + \sum_{k'} S_{k,nx;k',nx} A_{k',nx} + S_{k,nx;k,nx-1} A_{k,nx-1}, \\
& + S_{k,nx;k,nx+1} x_{k,nx+1} \alpha^{-1} \sum_{k'} x_{k',nx+1} A_{k',nx} \\
T_{k,k''} = & \sum_{k'} S_{k,nx;k',nx} B_{k',nx;k'',1} + S_{k,nx;k,nx-1} B_{k,nx-1;k'',1}, \\
& + S_{k,nx;k,nx+1} x_{k,nx+1} \alpha^{-1} \sum_{k'} x_{k',nx+1} B_{k',nx;k'',1}
\end{aligned} \tag{61}$$

Note that the actual value of the redshift has been nowhere specified and must be arranged by hand, as by choosing the initial trial orbits to have the input redshifts. However, the approximation  $\delta x_k/x_k \ll 1$  used to arrive at eq. (57) can fail, particularly in the first few iterations of the action, and so in practice the redshifts may drift away from their input values as the stationary point in the action is reached. This drift is corrected by periodically adjusting the particle positions at timestep  $nx + 1$  according to eq. (53).

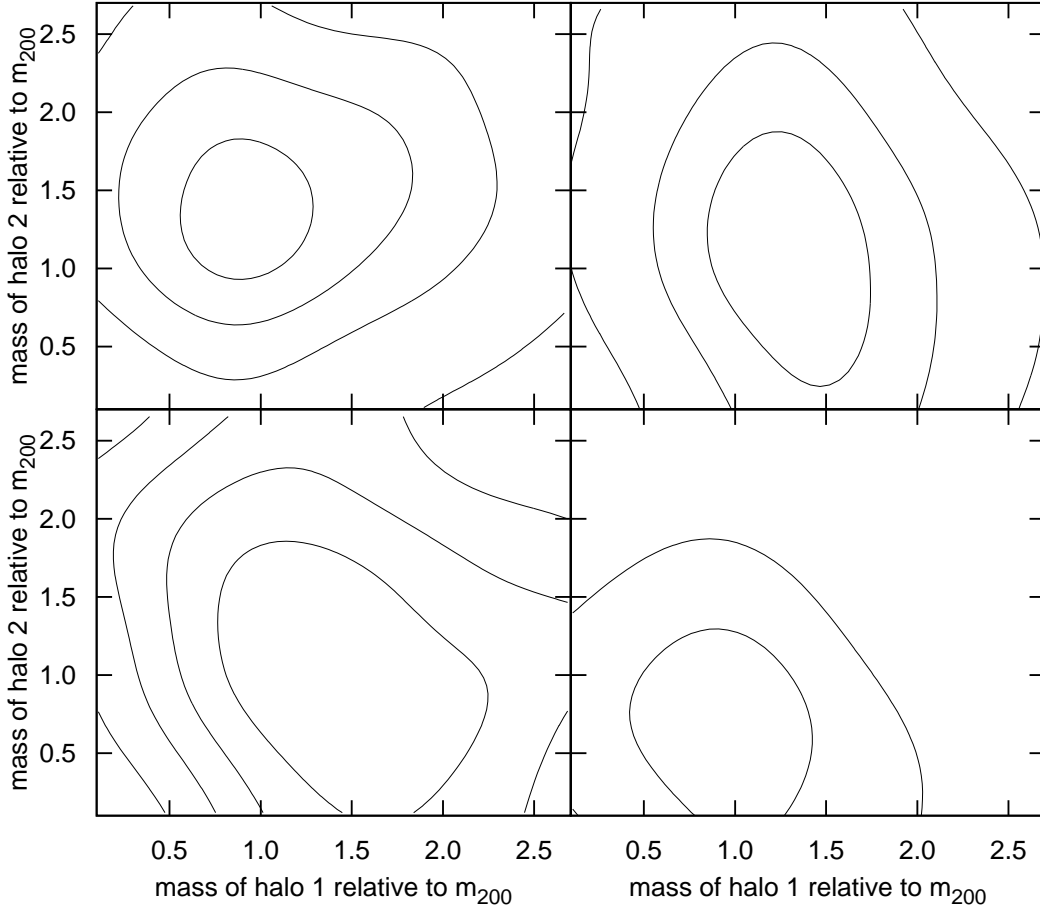
## REFERENCES

- Boylan-Kolchin, M., Bullock, J.S., Sohn, S.T., Besla, G., van der Marel, R.P. 2010, arXiv:1210.6046 [astro-ph].
- Bullock, J. S., 2012, arXiv:1009.4505 [astro-ph].
- Corteau, S., Van den Bergh, S., 1999, ApJ, 118, 337.
- Kahn F.D., Woltjer L. 1959, ApJ, 130, 705.
- Li, Y.S., White, S. 2008, MNRAS, 384, 1459.
- Peebles, P. J. E., 1989, ApJ, 344, L53.
- Peebles, P. J. E., 1995, ApJ, 449, 52.
- Peebles, P. J. E., Phelps, S. D., Shaya, E. J., and Tully, R. B., 2001, ApJ, 553, 2431.
- Peebles, P. J. E., Tully, R. B., Shaya, E. J., 2011, ApJ, 553, 2431.
- Peebles, P. J. E., Tully, R. B., 2013, arXiv:1302.6982 [astro-ph].
- Phelps, S. D., 2002, ApJ, 575, 1.
- Sohn S.T., Besla, G., Van der Marel, R.P., Boylan-Kolchin, M, Majewski, S.R., Bullock, J.S., 2012, arXiv:1210.6039 [astro-ph].
- Springel, V., White, S.D.M., *et al.* , 2005, Nature, 435, 629.
- van der Marel *et al.* , 2012, Apj, 753, 8.



..

Fig. 1.— Contours in  $\chi^2$  for different values of MW (x-axis) and M31 (y-axis) masses, for 4000 NAM solutions in four different scenarios. Upper left: results from the two-body problem of MW + M31. Upper right: LG actors only. Lower left: LG actors + 4 external groups. Lower right: same as lower left, with somewhat smaller initial guesses for the masses of the groups. The first contour level marks the region of 95% confidence (minimum  $\chi^2 +$



..

Fig. 2.— Contours in  $\chi^2$  for four different simulated Local Group catalogs. Each plot is generated from 4000 independent NAM solutions. Axes are unitless and represent the ratio of the NAM mass to the the actual halo mass in the simulation; thus the point at (1.0, 1.0) corresponds to a solution using the computed halo masses. The first contour level marks the region of 95% confidence (minimum  $\chi^2 + 6$ ).

Table 1: The Local Group catalog: observational constraints

Name	d	SGL	SGB	<i>cz</i>	<i>m<sub>cat</sub></i>
MW	0.00	0.00	0.00	0	22.5
M31	0.79	336.19	12.55	-119	25.1
Cen+	3.57	159.75	-5.25	386	119.0
M81+	3.66	41.12	0.59	72	70.6
Maff+	3.61	359.29	1.44	168	70.2
Scp+	3.58	271.56	-5.01	251	50.6
M33	0.92	328.47	-0.09	-45	1.97
LMC	0.05	215.80	-34.12	66	1.24
IC10	0.79	354.42	17.87	-150	0.434
NGC185	0.64	343.27	14.30	-40	0.106
NGC147	0.73	343.32	15.27	-4	0.077
NGC6822	0.51	229.08	57.09	43	0.06
LeoI	0.26	88.90	-34.56	121	0.001
LeoT	0.16	78.40	-38.75	-61	0.001
Phx	0.43	254.29	-20.86	-34	0.001
LGS3	0.65	318.13	3.81	-149	0.001
CetdSph	0.73	283.84	3.82	-27	0.001
LeoA	0.74	69.91	-25.80	-13	0.001
IC1613	0.75	299.17	-1.80	-159	0.001

units: Mpc, deg,  $\text{km s}^{-1}$ ,  $10^{11} M_{\odot}$ .